

# Neutron flux distribution in (Pb, Ta and W) target using accelerator of 18 MeV electron beam

Abdessamad Didi<sup>\*,1</sup>, Ahmed Dadoucha<sup>1</sup>, Otman Jai<sup>2</sup>,  
Mohamed Bencheikh<sup>1</sup>

<sup>1</sup>University of Sidi Mohamed Ben Abdellah, Fez, Morocco

<sup>2</sup>University Abdelmalak Saady, Tetouan, Morocco

\*e-mail: [abdessamad.didi1@usmba.ac.ma](mailto:abdessamad.didi1@usmba.ac.ma)

DOI: 10.29317/ejpfm.2018020205

Received: 09.05.2018

The production of neutrons can be carried out with the bombardment of the nuclei of heavy atoms, with accelerated and energetic particles (generally electrons). The electron collides with the target nuclei, so, 20 to 30 neutrons are produced by a process called "spallation". Several countries begin to develop neutron sources especially in the United States, Europe and Japan. The development of new measuring instruments and methods has generally increased the demand for neutron utilization in several areas, such as accelerator proton-based, where protons bombard a heavy metal target. The atoms of the target are excited, resulting in neutron emission.

**Keywords:** MCNP6; electron-beam, Am-Be; neutron flux; production of neutron.

## Introduction

This article focuses on the design of a spallation target in the electron accelerator system [1-3]. Monte Carlo simulations have been carried out with targets at varying thicknesses and diameters, bombarded by electron source particles with energy of (18 MeV). The neutron yields escaping from the outer surfaces of the targets were calculated and compared as a function of the beam energy of the target geometry and the target materials. In this study we kept the beam size 1 cm in diameter.

Due to the availability of nuclear data of photoneutron cross-sections [4], the application potential of spallation based on the electron accelerator increases [5] not only in medical applications [6-7], but also in other areas of research [8]. The subject of neutron yields from targets bombarded by electrons has been studied for many years [9-15]. This study describes the performance and nature of the target, design geometry, and size of target materials for a maximum neutron flux [15-16].

First, the photoneutrons converted by a target of heavy materials able of generating a beam of electrons into a neutron flux. Nevertheless, our article is devoted to the study of the design and to the optimization of the choice of the spallation target geometry for the generation of neutron flux.

The spallation system has been studied to find an optimal material used as a neutron converter. We performed several simulations with MCNP-6 using heavy

materials (Tantalum, Lead and Tungsten) [18-19]. The total neutron flux was calculated by varying the thickness and diameter of the target and the variation in the incident energy of the beams.

## Theory

### *Description of the matrix approach*

In order to obtain a large neutron flux, the study of the physical design of the targets is a mandatory condition. In this study, we tried to optimize the neutron flux by varying several parameters such as the geometry of the target and the energy of the beams. With the diameter and thickness variation of the target, we calculated the neutron flux exiting the surface of each cylinder indicated by a given thickness and diameters, in other words, the arithmetic variables of the target geometry vary according to the following matrix:

$$\begin{bmatrix} \varphi_{0,0} & \cdots & \varphi_{0,M} \\ \vdots & \ddots & \vdots \\ \varphi_{N,0} & \cdots & \varphi_{N,M} \end{bmatrix}$$

With  $i = 0, 1, \dots, M$  represents the maximum thickness of the target;

$j = 0, 1, \dots, N$  represents the maximum diameter of the target;

$\varphi$ : the neutron flux in each cylinder surface.

The neutron generation in the target materials was studied as a function of the accelerator energy, in order to evaluate the model based on the calculation of the matrix which represents the neutron flux in different types of targets (Lead, Tantalum and Tungsten) with dimensions  $9 \times 9$ .

$$\begin{pmatrix} \varphi_{00} & \varphi_{01} & \varphi_{02} & \varphi_{03} & \varphi_{04} & \varphi_{05} & \varphi_{06} & \varphi_{07} & \varphi_{08} \\ \varphi_{10} & \varphi_{11} & \varphi_{12} & \varphi_{13} & \varphi_{14} & \varphi_{15} & \varphi_{16} & \varphi_{17} & \varphi_{18} \\ \varphi_{20} & \varphi_{21} & \varphi_{22} & \varphi_{23} & \varphi_{24} & \varphi_{25} & \varphi_{26} & \varphi_{27} & \varphi_{28} \\ \varphi_{30} & \varphi_{31} & \varphi_{32} & \varphi_{33} & \varphi_{34} & \varphi_{35} & \varphi_{36} & \varphi_{37} & \varphi_{38} \\ \varphi_{40} & \varphi_{41} & \varphi_{42} & \varphi_{43} & \varphi_{44} & \varphi_{45} & \varphi_{46} & \varphi_{47} & \varphi_{48} \\ \varphi_{50} & \varphi_{51} & \varphi_{52} & \varphi_{53} & \varphi_{54} & \varphi_{55} & \varphi_{56} & \varphi_{57} & \varphi_{58} \\ \varphi_{60} & \varphi_{61} & \varphi_{62} & \varphi_{63} & \varphi_{64} & \varphi_{65} & \varphi_{66} & \varphi_{67} & \varphi_{68} \\ \varphi_{70} & \varphi_{71} & \varphi_{72} & \varphi_{73} & \varphi_{74} & \varphi_{75} & \varphi_{76} & \varphi_{77} & \varphi_{78} \\ \varphi_{80} & \varphi_{81} & \varphi_{82} & \varphi_{83} & \varphi_{84} & \varphi_{85} & \varphi_{86} & \varphi_{87} & \varphi_{88} \end{pmatrix}$$

### *Description method of Mesh tally*

The application of this technique is practically compatible with the majority of the Monte Carlo code. This method is based on the plotting of points using the results of the MCNP code, "Mesh-tally"; it is a graphical display of the particle flux (Voxel), and the distribution of the dose or other quantities on a rectangular, cylindrical or spherical grid superimposed at the top of the geometry of the standard problem. The particles are tracked through the independent mesh as part of the regular transport problem; and the content of each mesh was written in a DATA file at the end of the simulation. This file converts to a number of standard formats suitable for reading by different graphical analysis packages. The GRID-CONV conversion application that is provided in the MCNP package is a link that connects the MCNP "MDATA" calculation file with a graphical software. For

each mesh control card, it is necessary to have maps that give details of the mesh characteristics described as flux:

```

TMESH
RMESH1:n FLUX
CORAI -10.0 50i 10.0
CORBI -10.0 10.0
CORCI -10 50i 10
ENDMD

```

The target materials mentioned above are Lead, Tantalum and Tungsten, of cylindrical shape along the Z axis. The electron beam has an energy of 18 MeV and an electrical current equal to 10 mA bombards the targets at the zone surface area of each target used.

## Results and discussion

The results obtained from the surface flux matrix data and by mesh tally onto each surface of the each target study during the Monte-Carlo simulation, and shows an important rapport is that the surface flux connected logically with the studied parameters (Thickness, diameter and electron beams) as shown in the following table which shows the neutron efficiency characteristics as a function of thickness and diameter with 18 MeV beams.

### *Distribution in Lead Target*

Several variables are used to determine the optimal geometry of the target of lead, that is, the thickness and diameter of the target. Among the important parameters used in this study is the radius of the beam which is set at 0.5 cm. The 18 MeV energy electron beam bombards the cylindrical target at the lower center. The thickness varies with a 1 cm pitch along the target up to 8 cm; and the diameter of the target changes from 1 cm to 8 cm. The calculation error for the results obtained is less than 3%.

The total neutron flux on the surface of each cylinder has the lateral, lower and upper surfaces. It gives an overview of the neutron efficiency as a function of the diameter and thickness of the lead target (Figure 1), shows the neutron flux distribution as a function of the thickness and the diameter with an energy of electron beam of 18 MeV.

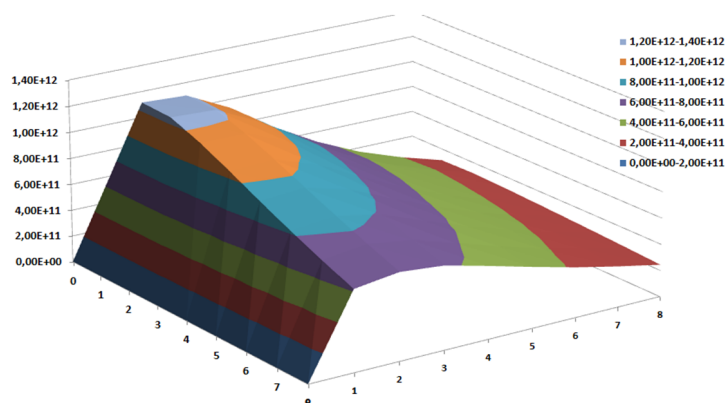


Figure 1. Neutron flux efficiency as a function of thickness and the target diameter of Lead under a 10 mA electron beam and an energy of 18 MeV.

The total neutron efficiency on all surfaces is the sum of neutron efficiency across the bottom surface, side surface and top surface. It gives an overview of the neutron efficiency as a function of the diameter and thickness of the lead target. The results mentioned in Figure 1 show that the flux is maximal when the thickness is between the values  $X = 1$  to 6 cm and the diameter between the values  $D = 1$  and 5 cm, in the two intervals. Concludes that the flux is between a maximum value of  $1.26 \times 10^{12}$  n/cm<sup>2</sup>s and a minimum value of  $9.48 \times 10^{11}$  n/cm<sup>2</sup>s.

From the results obtained, the zone of diameter of the optimum target must be about 2 cm and its thickness about 1.5 cm.

The following figure shows the neutron spectrum related to the neutron types involved in this study. The MCNP code gives the opportunity to give the neutron flux as a function of energy. Figure 2 shows the neutron distribution which defines the neutron flux as a function of energy.

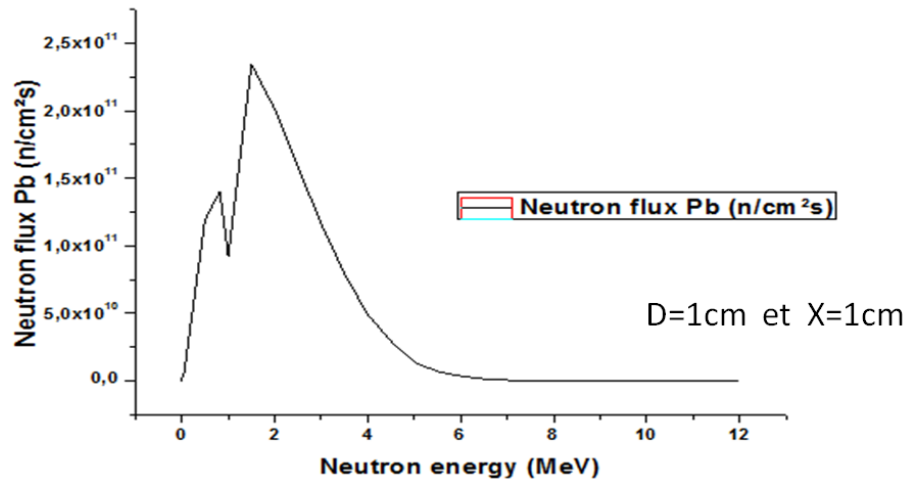


Figure 2. Neutron flux as a function of neutron energy in the lead target.

From the curve of Figure 2 where neutron flux is plotted as a function of neutron energy, a wide range of neutron energy of the Lead target is seen to have two very large peaks between  $2.5 \times 10^{-2}$  up to 7 MeV, which explains why lead is a target that can be useful for neutron production in particle accelerators. For the first peak of energy 0.821 MeV, the neutron flux is of the order of  $1.42 \times 10^{11}$  n/cm<sup>2</sup>s. For the second energy peak of 1.5 MeV the corresponding neutron flux is  $2.41 \times 10^{11}$  n/cm<sup>2</sup>s.

With the application of rectangular mesh, we divided the targets for three coordinates of  $(50 \times 50 \times 50)$ , yielding 125.000 points. For each point, the neutron flux.

We have calculated the axial flux which gives a maximum flux of the order of  $1.51 \times 10^{12}$  n/cm<sup>2</sup>s, and according to Figure 3, it can be seen that the maximum flux in the case of the thickness varying between 0.5 and 2.5 cm of the target of lead and of diameter between 0 and 2 cm. Then the intensity of the neutron flux decreases as a function of thickness and diameter, and the change of color from inside to outside explains the change in the intensity of the flux.

The radial flow expressed in Figure 4 clearly explains that the intensity of the neutron flux in the lead target is symmetrical with respect to the X axis and maximum in the diameter between 0 and 2 cm.

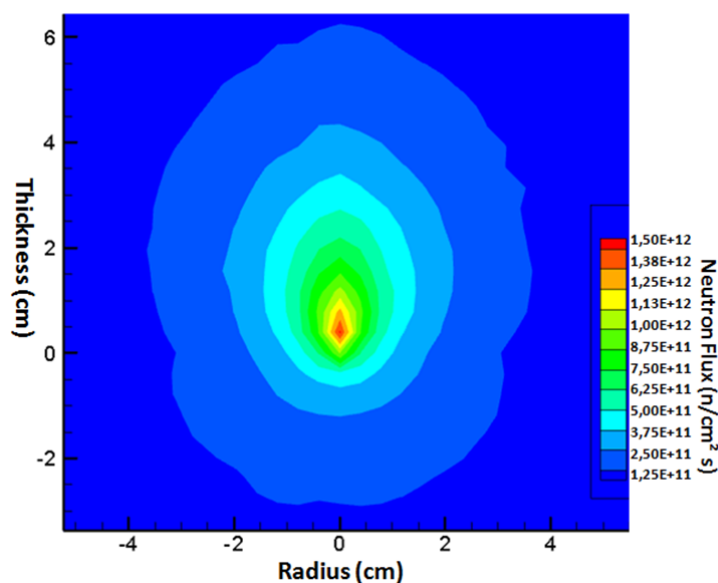


Figure 3. Axial neutron flux distribution of the Pb target driven by a 10 mA electron beam and an energy of 18 MeV.

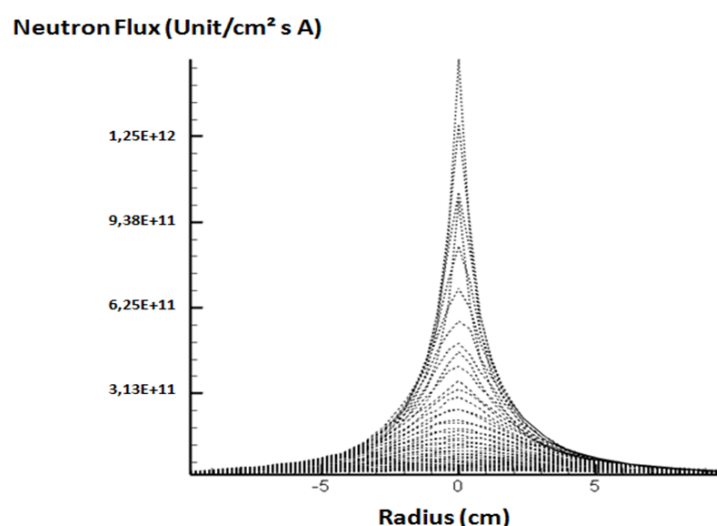


Figure 4. Radial neutron flux distribution of the Pb target driven by a 10 mA electron beam and an energy of 18 MeV.

### *Distribution in the Tantalum target*

The same variables are applied in the Tantalum study to determine the optimal geometry of the target used as a spallation system. First, the thickness and diameter of the target, and then the 18 MeV electron beam bombarding the Ta target. The other data remain fixed to compare the results found with Lead (the size of the beam was fixed at 1 cm, the thickness varies with a step of 1 cm along the target up to 8 cm and the diameter of the target changes 1 cm, 2 cm, 3 cm, 4 cm, up to 8 cm). The calculation error for the results obtained is less than 3%.

After the calculation has been made, the neutron flux on the surface of each cylinder has the lateral, lower and upper surfaces. The figure shows that the neutron efficiency varies remarkably as a function of the diameter and the thickness of the Tantalum target. Figure 5 shows the neutron flux distribution as a function of thickness and diameter with electron beam energy of 18 MeV.

The results mentioned in Figure 5 show that the flux is maximal when the thickness comprises the values  $X = 1$  to 4 cm and the diameter the values of  $D = 1$  and 4 cm. In the field of the results selected in this interval, the maximum

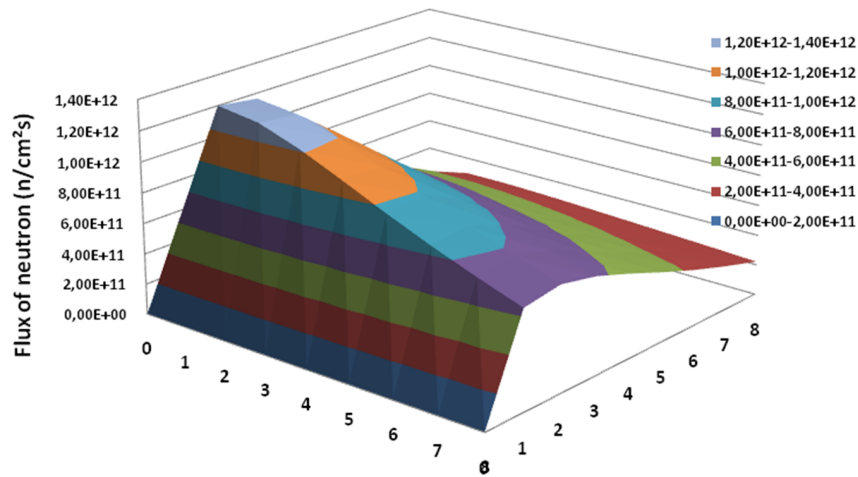


Figure 5. Neutron flux efficiency as a function of thickness and the target diameter of Tantalum under a 10 mA electron beam and an energy of 18 MeV.

flux is of the order of  $1.32 \times 10^{12}$  n/cm<sup>2</sup>s and the minimum value is  $8.48 \times 10^{11}$  n/cm<sup>2</sup>s. According to the results obtained, the zone of optimum diameter of the target is 2 cm and the thickness of the optimal target is 1 cm.

The spectrum of the neutron flux whose diameter is 1 cm and the thickness of 1 cm of the target as a function of the neutron energy is shown in Figure 6.

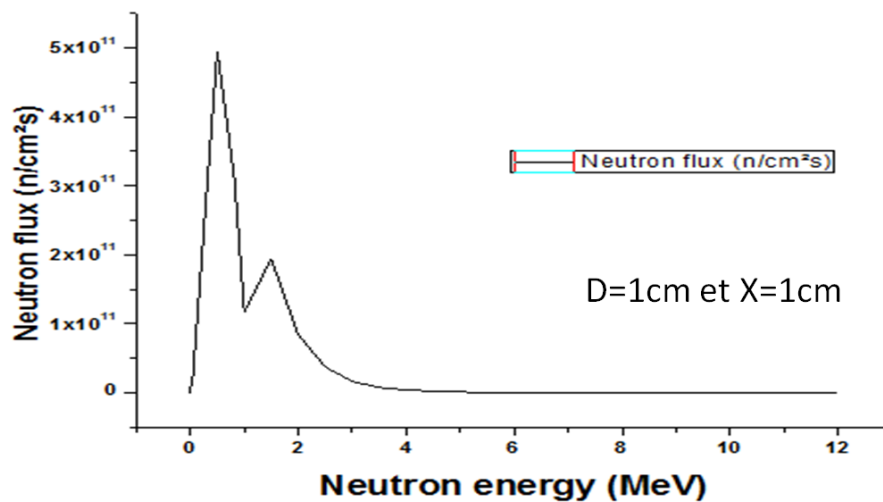


Figure 6. Neutron flux as a function of neutron energy in the lead target.

From the analysis in Figure 6, we observe that when a Tantalum target is bombarded by an electron beam, the phenomenon of photoneutron ( $\gamma, n$ ) takes place, the type of neutron produced is in the energy range of  $10^{-1}$  up to 4 MeV, which means that the majority of neutrons are of a fast nature. The peak of  $10^{-1}$  MeV gives a flux of  $3.05 \times 10^{11}$  n/cm<sup>2</sup>s.

The calculated axial neutron flux is about  $1.63 \times 10^{12}$  n/cm<sup>2</sup>s, in this Figure 7 there is a change in color which means changes in the intensity of the flow. The optimum geometry according to the results found is placed 0.5 and 2 cm in thickness and 0 to 2 cm in diameter.

The radial neutron flux symmetrical with respect to the X axis is maximum at the medium; a maximum flux peak of the order of  $1.58 \times 10^{12}$  n/cm<sup>2</sup>s, then decreases symmetrically on both sides. In Figure 8, it is noted that the diameter

at 2 cm is an optimum diameter which gives a maximum flow.

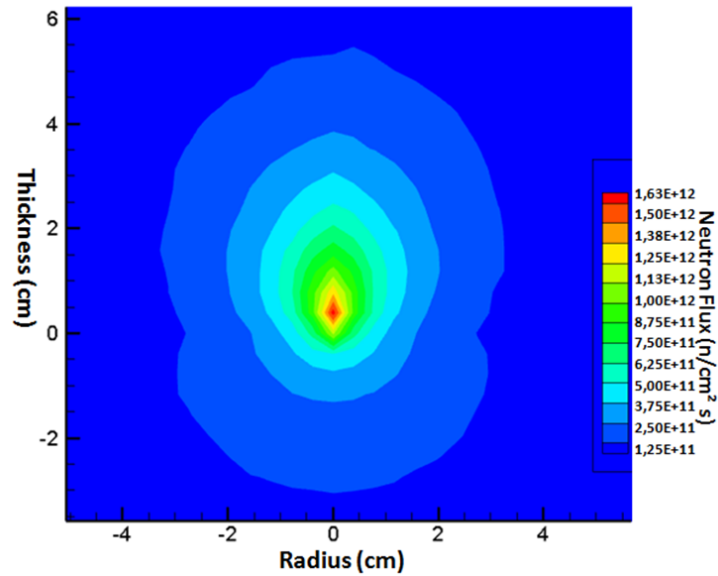


Figure 7. Axial neutron flux distribution of the Ta target driven by an electron beam of 10 mA and an energy of 18 MeV.

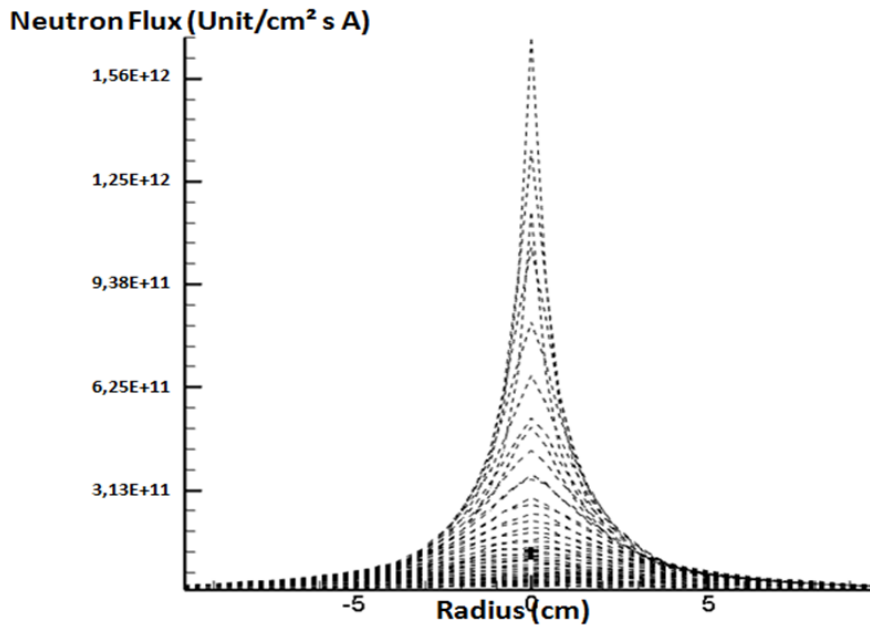


Figure 8. Radial neutron flux distribution of the Ta target driven by an electron beam of 10 mA and an energy of 18 MeV.

### *Distribution in Tungsten Target*

Tungsten is the third target exposed to an electron beam of 10 mA and 18 MeV. The matrix clearly shows that the neutron flux varies as a function of thickness and diameter. After the calculation of neutron fluxes on all the surfaces binding each diameter to a given thickness of  $W$ . Figure 9 shows that the neutron flux changes exponentially as a function of the thickness and diameter of the target.

The curve gives an accuracy on the surface neutron flux of each surface framed by a diameter and a thickness of the target of  $W$ . The total neutron flux in the thickness is between the values  $X = 1$  to 4 cm and the diameter between the values of  $D = 1$  and 3 cm. The flux of  $1.3 \times 10^{12}$  n/cm<sup>2</sup>s has a maximum value and  $8.98 \times 10^{11}$  n/cm<sup>2</sup>s as the minimum value.

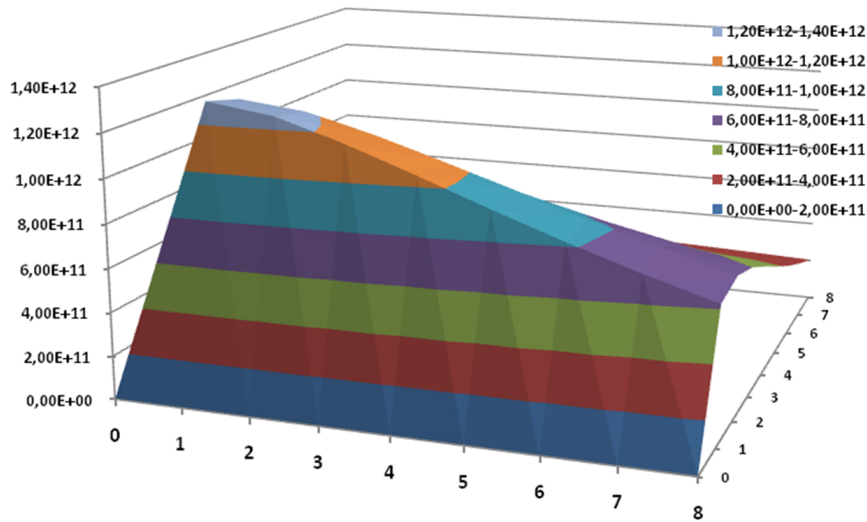


Figure 9. The neutron flux efficiency as a function of the thickness and the target diameter of Tungsten under a 10 mA electron beam and an energy of 18 MeV.

From the results obtained, the zone of diameter and the optimum thickness of the target are in the vicinity of 1 cm.

After the analysis of the neutron flux spectrum Figure 10, in the case where the geometry of the target of W is 1 cm in diameter and thickness as a function of the neutron energy. The spectrum of Tungsten is obtained at the energy of 0.5 MeV. The peak has the same characteristics as the Tantalum target with some variation in the flux Tungsten gives more neutrons than the Tantalum. It can be explained that the W and Ta are two elements of Z closer to each other by adding to lead (Pb) which has a larger Z, which explains their large neutron flux.

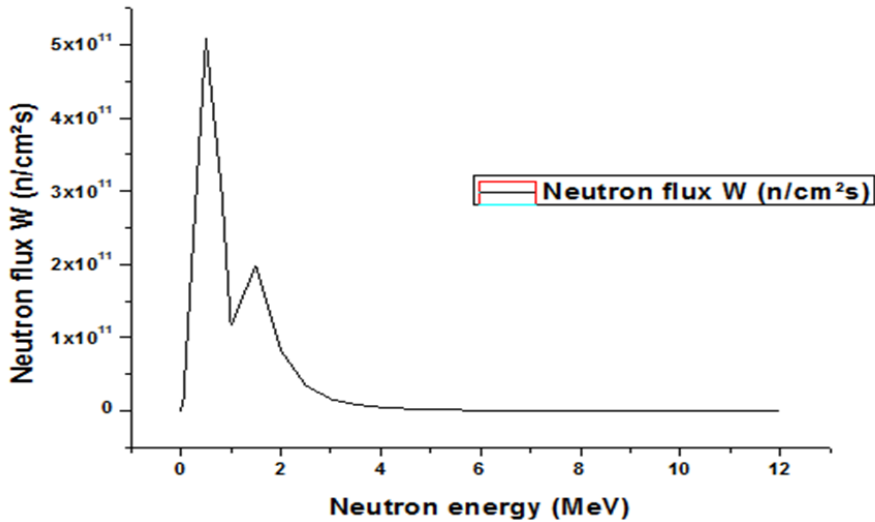


Figure 10. The neutron flux as a function of neutron energy in the Tungsten target.

The flux of the electron source beam gives a neutron flux of  $1.75 \times 10^{12}$  n/cm<sup>2</sup> s. Figure 11, using the meshing method.

Figure 12 represents the radial neutron flux which is of the order of  $1.56 \times 10^{12}$  n/cm<sup>2</sup> s, the symmetrical flux by contribution to the x = 0 axis, the flux rapidly deprived on both sides of the origin.

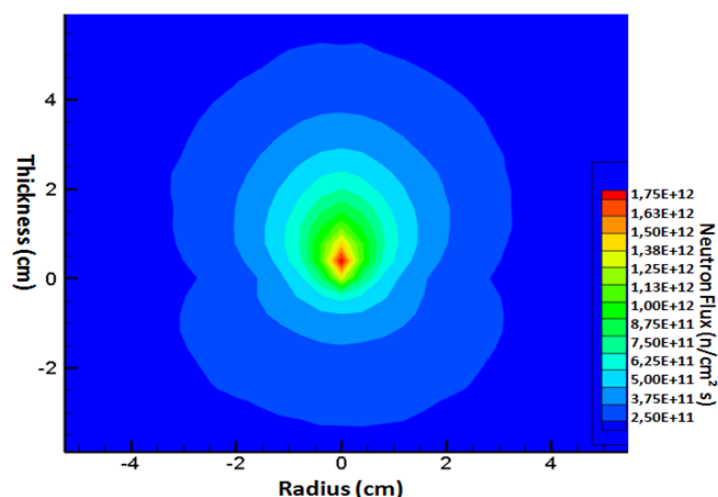


Figure 11. Axial neutron flux distribution of the W target, driven by a 10 mA electron beam and 18 MeV energy.

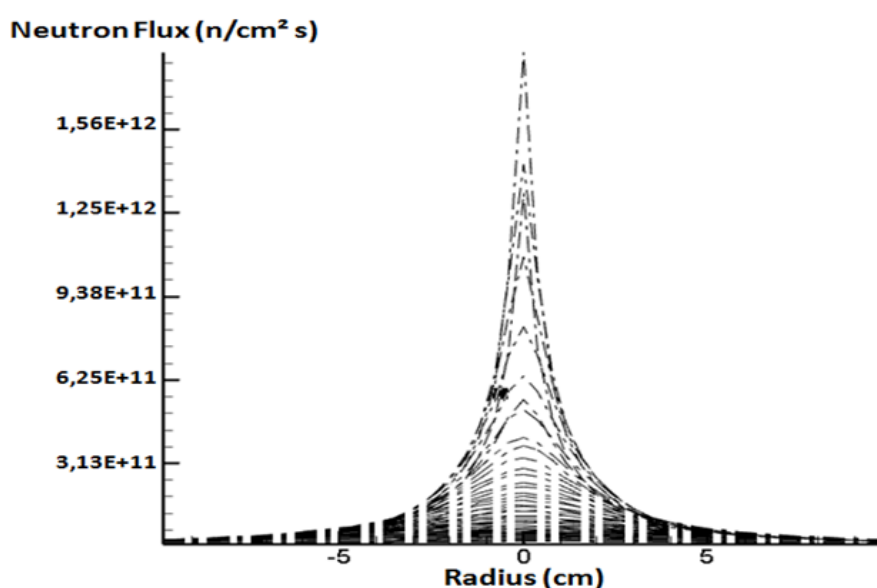


Figure 12. Radial neutron flux distribution of the W target, driven by a 10 mA electron beam and 18 MeV energy.

## Conclusion

The production of neutrons using a spallation source based on an electron accelerator, explained previously, is done via the photo-neutron interaction. However, a 10 mA electron beam with an energy of 18 MeV can generate a neutron flux of different energy ranges for different targets (Lead, Tantalum and Tungsten). The intensity of the neutron flux varies according to the thickness and diameter of the target (geometry).

Since all the calculations made, Table 1 shows the results of different fluxes produced (Photon, Neutron and total flux) for a 10 mA electron beam that bombards the targets (Pb, Ta and W). Table 1. Maximum neutron, photon and total fluxes for Pb, Ta and W with an electron-based accelerator of 10 mA and an energy of 18 MeV

It has been estimated that an 18 MeV electron beam-driven accelerator produces a maximum neutron flux generated by the spallation targets (Pb, Ta and W) is  $1.26 \times 10^{12}$ ,  $2.63 \times 10^{12}$  and  $1.301 \times 10^{12}$  (n/cm<sup>2</sup> s) using the matrix method.

Then, the estimated values of the maximum photon flux calculated for the same targets, give the following results:  $1.438 \times 10^{15}$ ,  $1.221 \times 10^{15}$  and  $1.158 \times 10^{15}$  (unit/cm<sup>2</sup>s). It has been observed that the flux has varied according to the target and its geometry. Lead has been shown to give the maximum flux among all the targets considered. The results are consistent with the results obtained by the meshing method where the flux gives the following results:  $1.50 \times 10^{12}$ ,  $1.63 \times 10^{12}$  and  $1.75 \times 10^{12}$  (n/cm<sup>2</sup>s).

Table 1.

Maximum neutron, photon and total fluxes for Pb, Ta and W with an electron-based accelerator of 10 mA and an energy of 18 MeV.

	Electrons Beam (MeV)	Pb	Ta	W
Photon flux (unit/cm <sup>2</sup> s)	18 MeV	$1.438 \times 10^{15}$	$1.221 \times 10^{15}$	$1.158 \times 10^{15}$
Neutron flux (unit/cm <sup>2</sup> s)	18 MeV	$1.26 \times 10^{12}$	$2.63 \times 10^{12}$	$1.301 \times 10^{12}$
Total (unit/cm <sup>2</sup> s)	18 MeV	$1.439 \times 10^{15}$	$1.222 \times 10^{15}$	$1.160 \times 10^{15}$

The neutron generation is performed by several parameters, including target materials, target size, beam energy, and beam size. Optimization of the neutron flux by the matrix or mesh approach gives acceptable results to obtain a maximum flux of optimum thickness and diameter of 1 cm respectively.

The generation of neutrons from the target is not only related to the neutron flux distributions, but also to the distributions of the source particle beams. In the previous section concerning the neutron flux distribution and the neutron generation from the targets, we have focused our research on the flux distribution for different bombarded targets by electrons.

## References

- [1] G. Glinatsis et al., *Annals of Nuclear Energy* **104** (2017) 1.
- [2] Meigo, Shin-ichiro, *Journal of Nuclear Materials* **450** (2014) 8.
- [3] Abdessamad Didi et al, *Der Pharmacia Lettre* **9** (2017) 107.
- [4] P. M. Milazzo et. al., *Nuclear Instruments and Methods in Physics Research Section B: Beam Interactions with Materials and Atoms* **213** (2004) 36.
- [5] T. Goorley, Initial MCNP6 Release Overview MCNP6 Version 1.0, LA-UR-13-22934, Los Alamos National Laboratory (2013).
- [6] F. Tabbakh, *J. Nuc. Rela. Tech* (2012) 48.
- [7] N.P. Dikiy, *Proceed. of Joint Accelerator Conf.*, Stockholm (1998) 2389.
- [8] Y. Liu, *Dissertation, Raleigh North Carolina* (2006) 189 p.
- [9] J. M. Berger, *Phys Rev.* **105** (1957) 35.
- [10] U. Kneissl, *Nucl Phys. A* **247** (1975) 91.
- [11] J. Pottier, *Nuc. Instr. Methods Phys. Rese. B* **40/41** (1989) 943.
- [12] G. N. Kim, *J. Accel. Plasma Res.* **3** (1998) 9.
- [13] I. Akkurt et al., *Phys. in Med. and Biol.* **48**(20) (2003) 3345.
- [14] E. Haug, *Astron. Astro. Phys.* **406** (2003) 31.

- [15] J. Chen, Accelerator-Driven Sub-critical System Characterization, s.l.: ADSS Experiments Workshop (2006).
- [16] F. Rahmani, App. Rad.Isotopes **106** (2015) 45
- [17] W. L. Huang, Nucl. Instrum. Methods Phys. Res. B **229** ( 2005) 339.
- [18] J. Martin Berger, Phys. Rev. C **2** (1970) 621.
- [19] S. M. Seltzer, Phys.Rev. C **7** (1973) 858.